NASA Technical Memorandum 106894

Electric Field Effects on a Near-Critical Fluid in Microgravity

G. Zimmerli
NYMA, Inc.
Engineering Services Divsion
Brook Park, Ohio

R.A. Wilkinson
National Aeronautics and Space Administration
Lewis Research Center
Cleveland, Ohio

R.A. Ferrell and H. Hao
University of Maryland
College Park, Ohio

M.R. Moldover
National Institute of Standards and Technology
Gaithersburg, Maryland

Prepared for the
National Heat Transfer Conference
sponsored by the American Society of Mechanical Engineers
Portland, Oregon, August 5–9, 1995

Corrected Copy

National Aeronautics and
Space Administration

Electric Field Effects on a Near-Critical Fluid in Microgravity

G. Zimmerli
NYMA, Inc.
Engineering Services Division
Brook Park, Ohio 44142

R.A. Wilkinson
National Aeronautics and Space Administration
Lewis Research Center
Cleveland, Ohio 44135

R.A. Ferrell and H. Hao
University of Maryland
Department of Physics
College Park, Maryland 20742

M.R. Moldover
National Institute of Standards and Technology
Thermophysics Division
Gaithersburg, Maryland 20899

ABSTRACT

We have studied the effects of an electric field on a sample of SF_6 fluid in the vicinity of the liquid-vapor critical point. We measured the isothermal increase of the density of a near-critical sample as a function of the applied electric field. In agreement with theory, this electrostriction effect diverges near the critical point as the isothermal compressibility diverges. Also as expected, turning on the electric field in the presence of density gradients can induce flow within the fluid, in a way analogous to turning on gravity. These effects were observed in a microgravity environment by using the Critical Point Facility which flew onboard the Space Shuttle Columbia in July 1994 as part of the Second International Microgravity Laboratory Mission. Both visual and interferometric images of two seperate sample cells were obtained by means of video downlink. The interferometric images provided quantitative information about the density distribution throughout the sample. The electric field was generated by applying 500 V to a fine wire passing through the critical fluid.

INTRODUCTION

Although there has been a great deal of work done in the study of electric field effects in fluids, experimental investigations of electric field effects near critical points has been limited to experiments involving binary liquid mixtures (Debye and Kleboth, 1965, Wirtz and Fuller, 1993, and Yosida, 1978). One difficulty that arises when studying the effects of an applied electric field on near-critical binary liquid mixtures is that the electrical conductivity of the fluid leads to heating effects. Even though the conductivity of the binary mixture may be small, the required electric fields are high enough that ohmic heating is significant. Near a critical point, the thermodynamic properties of the system vary rapidly as the temperature approaches the critical temperature. Heating the fluid takes the system away from the critical point, thereby disturbing the measurements.

In the present study, we report our measurements of the electrostriction effect in a single-component nonconducting fluid, sulfur hexaflouride (SF_6), near the liquid-vapor critical point. Electrostriction is the deformation of a fluid or solid in the presence of an electric field. Near a critical point, the electrostriction effect becomes more pronounced because the compressibility diverges. To our knowledge, these are the first reported measurements of electrostriction near a critical point. We shall also discuss our observations of the dielectrophoretic force on the SF_6 fluid in a microgravity environment.

In order to understand the need for an extended duration microgravity environment, it is helpful to begin with a brief discussion of some thermodynamic properties near the liquid-vapor critical point.

The critical point of a fluid marks the endpoint of the liquid-vapor coexistence curve in the pressure-temperature plane, and is uniquely characterized by a critical temperature T_c, critical density ρ_c, and critical pressure P_c. For SF_6, the critical point occurs at $T_c = 318.69$K, $P_c = 3.76$ MPa and $\rho_c = 0.73$ g/cc. As the critical point is approached, fluctuations in the fluid density occur at increasingly longer length and time scales. The size of the density fluctuations are characterized by the correlation length ξ, which diverges according to the power-law expression (Sengers and Sengers, 1978)

$$\xi = \xi_0 T_*^{-\nu} \tag{1}$$

as the critical point is approached from above T_c. Here, $T_* = (T - T_c)/T_c$ is the reduced temperature, ξ_0 is the correlation length amplitude (for SF_6, $\xi_0 = 0.2$ nm), and $\nu = 0.63$ is the critical exponent characterizing the strength of the divergence. One of the most dramatic consequences of the diverging correlation length is the increase in scattered light from the fluid. Close to the critical point the correlation length becomes comparable to the wavelength of visible light, resulting in strong scattering and a corresponding increase in turbidity.

Many of the fluid properties exhibit singular behavior at the critical point. For example, the specific heats at constant volume c_v and constant pressure c_p, the isothermal compressibility K_t, and thermal

conductivity Λ are all diverging quantities. Because of the fact that c_p diverges faster than Λ, the thermal diffusivity, D_t, given by

$$D_t = \Lambda / \rho c_p \tag{2}$$

approaches zero as the critical point is approached. A numerical expression for the thermal diffusivity of SF_6 which accounts for both the critical part of the diffusivity and the background diffusivity far from T_c is

$$D_t\left(T_*\right) = 1.39 \cdot 10^{-2} \cdot T_*^{1.24} + 2.08 \cdot 10^{-4} \cdot T_*^{0.61} \tag{3}$$

and has units of cm^2/sec. We have obtained Eq. 3 by fitting to Jany and Straub's (Jany and Sraub, 1987) light scattering data on SF_6.

Because the density fluctuations decay away at a rate proprotional to D_t, the lifetime of fluctuations increases as one gets closer to T_c. This has important consequences for an experiment; a small temperature or density disturbance in the fluid slowly decays back to equilibrium via thermal diffusion. The time constant associated with thermal diffusion is

$$\tau = l^2 / \pi^2 D_t \tag{4}$$

where l is a characteristic length of the container. In these experiments, τ was as much as several hours close to T_c. This phenomena of increasing relaxation times close to T_c is known as critical slowing down. Although adiabatic effects can speed up the heat transfer process (Onuki, et al., 1990 and Boukari, et al., 1990) the late stages of relaxation are still governed by the time constant τ. Depending on the amplitude of the initial disturbance, one may have to wait several time constants before reaching true equilibrium.

The isothermal compressibility $K_t = -1/V(dV/dP)_T$ of a fluid at the critical density diverges near the critical point as

$$K_t = \frac{\Gamma T_*^{-1.24}}{P_c} \tag{5}$$

where Γ = 0.0459, in the restricted cubic model (Sengers and Sengers, 1978 and Moldover, et al., 1979) for SF_6. Close to T_c, the high compressibility leads to density stratification in the earth's gravitational field. For a fluid such as SF_6., the density stratification becomes significant within 30 mK of T_c. At T_c itself, the density at the bottom of a 1 cm-tall sample of SF_6 will exceed the density at the top by 8%. Moldover et al., have reviewed gravity effects in fluids near the critical point (Moldover, et al., 1979). A long duration low-gravity environment will avoid gravity-induced stratification and make it possible to study critical fluids closer to T_c than on earth.

ELECTRIC FIELD EFFECTS

In the absence of free charge, and neglecting the effect of gravity, the force acting on a unit volume element of dielectric in an electric field of strength E is given by (Stratton, 1941)

$$\mathbf{f} = -\frac{1}{2} E^2 \nabla(\varepsilon) + \frac{1}{2} \nabla\left(E^2 \rho d\varepsilon / d\rho\right) \tag{6}$$

where ε is the permittivity. The first term is known as the dielectrophoretic force and the second term represents the force due to electrostriction.

The dielectrophoretic force arises from spatial gradients in the permittivity. In the case of fluids, the permittivity is a function of density via the Clausius-Mossotti relation. Thus, density gradients will be affected by the dielectrophoretic force. The dielectrophoretic force is usually quite weak in comparison with gravity. However, in a microgravity environment, the dielectrophoretic force can pump and confine liquids (Melcher and Hurwitz, 1967) and it can induce convective flows (Hart, et. al., 1986). The possibility of using strong electric fields to counter the gravity induced density stratification which occurs near the critical point was recognized over 25 years ago (Voronel and Gitterman, 1969). Fields of tens of kilovolts/cm are required.

The electrostriction term in Eq. 6 contributes to an electrostrictive pressure. Stratton (1941) shows that the increase in pressure due to the electric field relative to a point in the fluid where $E = 0$ is given by

$$\Delta P = \varepsilon_0 E^2 (\kappa - 1)(\kappa + 2)/6 \tag{7}$$

where ε_0 is the vacuum permittivity and $\kappa = \varepsilon/\varepsilon_0$ is the relative dielectric constant (κ = 1.28 for SF_6 at the crititcal density). The isothermal increase in density associated with the increased pressure is then

$$\Delta\rho / \rho = \varepsilon_0 K_t E^2 (\kappa - 1)(\kappa + 2)/6 \tag{8}$$

This represents the density increase for a system in contact with a large pressure resevoir; for example, two small electrodes forming a capacitor in a much larger fluid volume.

Since the compressibility of a fluid is often negligible, the electrostriction effect is usually neglected. In the case of a critical fluid, however, the isothermal compressibility is diverging as the critical point is approached. Upon applying the electric field, we do not expect to see the immediate full change in the density given by Eq. 8 since it represents an isothermal result. In fact, turning on the electric field will heat the fluid a small amount due to the electrocaloric effect (Landau and Lifshitz, 1984). The excess heat gradually diffuses out of the fluid, and the fluid returns to the original temperature after approximately a thermal diffusion time constant τ. The immediate, or adiabatic, density change would be given by Eq. 8 with the substituion of the adiabatic compressibility $K_S = (c_p/c_v)^{-1} K_t$ for the isothermal compressibility. Since the ratio c_p/c_v diverges near the critical point ($c_p/c_v = 730$ at $T_c + 100$ mK for SF_6), the adiabatic density change was too small for us to detect close to T_c ; however, the isothermal change was easily measured.

Another point which we must consider is the effect of the electric field on the critical point. Landau and Lifshitz (1984) show that an electric field shifts the critical temperature and critical density of the fluid. Voronel and Gitterman (1969) estimate the shift in T_c to be about 1 mK for a typical fluid subjected to a field of 45 kV/cm. Thus, the effect could be important very close to T_c under high electric fields.

EXPERIMENTAL RESULTS

The experiment was carried out using the Critical Point Facility (CPF) (Cork, et. al., 1993) which flew on the Second International

Microgravity Laboratory (IML-2) during the STS-67 flight of Columbia in July, 1994. The CPF is a multi-user instrument designed and built in Europe, and operated by the European Space Agency. Five seperate experiments were conducted on CPF during the IML-2 mission. Each individual experiment has its own thermostat which could be changed out of CPF by the shuttle crew members to initiate the start of a new experiment. CPF has the capability to view both an interferometer cell and a visualization cell.

A schematic of the fluid region of our interferometer (IF) cell is shown in Fig. 1. The fluid volume of the IF cell is bounded by a stainless steel spacer and quartz windows. The inside diameter of the spacer is 12 mm, and its thickness is 2 mm. A 1 mm thick semi-circular quartz "button" was attached to one window. This reduces the height of the fluid to 1 mm in half of the cell. A 0.127 mm diameter wire runs through the 2 mm thick section of the fluid, parallel to the edge of the quartz button and approximately 1.5 mm away from its edge. The wire was spot welded to electrical feedthroughs which in turn were epoxied into the spacer. The electric field was generated by applying a voltage to the wire.

The IF cell comprises one leg of a Twyman-Green interferometer. A multi-layer dielectric mirror coating was applied to the inner surface (in contact with the fluid) of one of the windows. Both surfaces of the other window had anti-reflection coatings. In addition, both inner surfaces were coated with a conductive, transparent indium-tin-oxide coating to eliminate effects from static charges which may otherwise accumulate. The conductive coatings made electrical contact to the spacer via the gold o-rings which were used to seal the cell. The spacer was kept at ground potential throughout the experiment. The design of the visualization cell differed slightly from that of the IF cell. There was no quartz button in the cell and the fluid filled space between windows was 1 mm. The windows were coated only with the conductive coating, and were kept at ground potential. Both sample cells were filled to within 0.3% of the critical density with 99.999% pure SF_6.

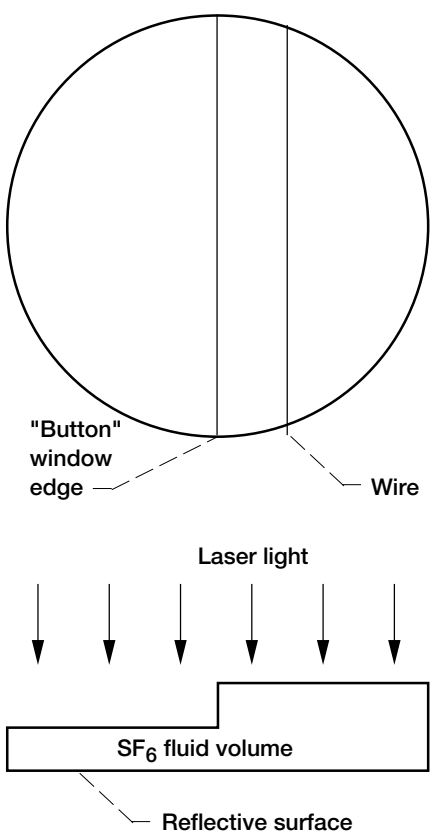

Figure 1.—Top view and cross-section of the interferometer sample cell fluid volume which was filled with SF_6 at the critical density. The diameter of the fluid volume is 12 mm. An electric field is created in the fluid by charging the wire to 500 V.

During the experiment, either sample cell could be viewed by a command to CPF to open or close appropriate shutters. The sample cells were imaged by a CCD camera which typically recorded one frame every six seconds. The digital image was sent to the ground, recorded and displayed. The 6 bit resolution of the CCD provided 64 gray levels and a spatial resolution of 40 μm at the focal plane. Unfortunately, the interferometer channel was not focused at the IF cell. During the experiment, commands from the ground to CPF were used to turn the voltage on and off, take high resolution still photographs, and change the set-point of the thermostat. At a given setpoint temperature, the long-term temperature stability was better than 0.1 mK.

Changes in the fluid density distribution were measured by monitoring changes in the interferometric fringe pattern, which sensed changes in the optical path length. The optical path length of the laser light in the fluid is $N\lambda = 2ln$ where N is the number of wavelengths which make a double pass through the fluid, λ is the wavelength of the light (633 nm), l the thickness of the fluid (1 or 2 mm) and n the index of refraction of the fluid (n =1.092 for SF_6 at the critical density). A change in the fluid density changes the optical path length and hence the fringe pattern. The resulting fringe shift ΔN is found by differentiation to be

$$\Delta N = (2l/\lambda)(\delta\rho/\rho)n' \tag{9}$$

where $\delta\rho$ is the density change of interest and

$$n' = \rho\, dn/d\rho = \left(n^2 - 1\right)\left(n^2 + 2\right)\Big/6n \tag{10}$$

is obtained from the Lorentz-Lorenz relation which relates density to index of refraction. A relative density change of 0.01% in the 2 mm thick section of our fluid sample would thus produce a fringe shift ΔN = 0.058 fringes which was roughly the limit of our resolution. For a homogeneous density distribution, the fringe pattern is determined by the amount of tilt in the reference mirror of the interferometer together with any distortions resulting from the optics. Figure 2(a) shows the equilibrium fringe pattern obtained at T_C +1 K with the electric field off. The bending of the fringes around the edges of the cell is due to bowing in the quartz windows which results from the forces needed to seal the cell. A discontinuity in the fringe pattern is visible across the diameter of the cell. This is a result of the semi-circular quartz button, which changes the optical path length relative to the other half of the cell.

Figure 2(b-d) shows the equilibrium fringe pattern obtained with the wire charged to a potential of 500 V at T_C + 30 mK, T_C + 10 mK, and T_C + 5 mK respectively. The bending of the fringe pattern near the wire, especially visible in Figs. 2(c) and (d), is a result of the density increase near the wire due to electrostriction. As explained previously, turning on the electric field generates a small amount of heat which must diffuse out of the fluid. Thus, to reach

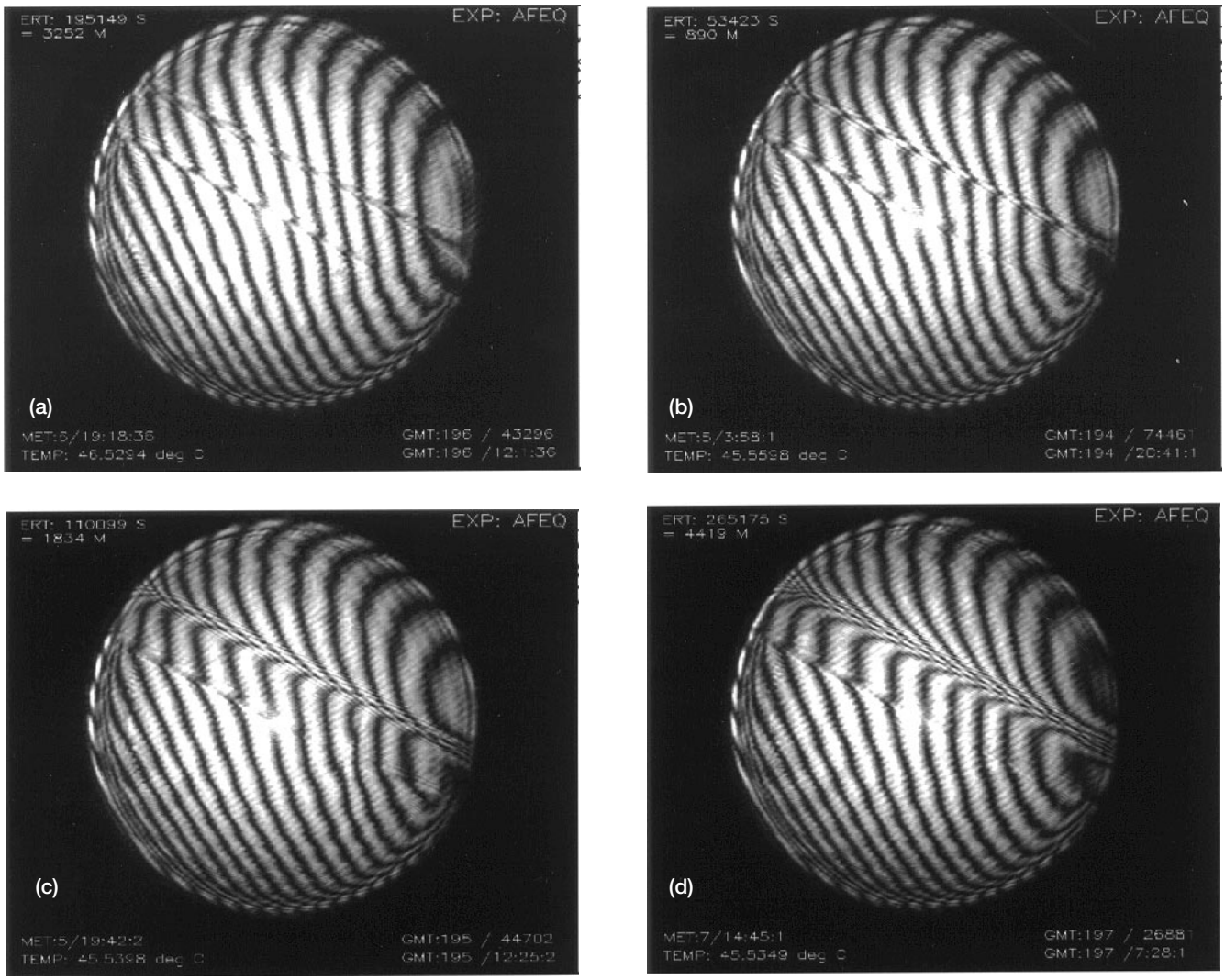

Figure 2.—Interferograms of the SF_6 fluid in a low-gravity environment. The bending of the fringes near the wire signifies the density increase due to the electrostriction effect. (a) T_c+1 K with no electric field. (b) T_c+30 mK after 3 hr at 500 V. (c) T_c+10 mK after 6 hr at 500 V. (d) T_c+5 mK after 14 hr at 500 V.

isothermal conditions it is necessary to wait at least a diffusion time constant for the fluid to reach equilibrium. The fringe patterns shown in Figs. 2(b-d) were obtained after leaving the 500 V potential on for 3, 6, and 14 hr respectively.

Figure 2 shows that the fringe shift increases as T_C is approached. This is consistent with Eqs. 5, 8 and 9 which show that ΔN is proportional to the compressibility which, in turn, diverges as the critical point is approached. A detailed analysis of the fringe pattern will appear in a separate publication. Here, we give a simple, order-of-magnitude estimate of the expected fringe shift.

The electric field between two coaxial conductors is

$$E(r) = V_o \big/ \big(r \ln(b/a)\big) \tag{11}$$

where r is the radial distance from the center, a is the radius of the inner conductor, b is the radius to the outer conductor and V_o is the potential difference between the inner and outer conductors. For our cell geometry, a = 0.064 mm and we note that the distance to the ground plane ranges from 1 mm to about 4.5 mm in the 2 mm thick fluid section. We shall use ln (b/a) = 3.5 in our simplified analysis which is within 20 percent of the value calculated using either b = 1 mm or b = 4.5 mm. Next, we note that the interferometer integrates the density (or optical path) along the direction perpendicular to the windows which we shall call the y direction. To calculate the fringe shift, we must integrate the electric field along the y coordinate. Combining Eqs. (5), (8), (9), and (11) we find the fringe shift a perpendicular distance x_0 away from the center of the wire is

$$\Delta N = \frac{\varepsilon_0 \, K_t \, n'}{3\lambda}(\kappa - 1)(\kappa + 2)\int dy \, E^2$$

$$\cong 2 \cdot 10^{-7} T_*^{-1.24}\left(1/x_0\right)\tan^{-1}\left(1/x_0\right) \tag{12}$$

where we have substituted values appropriate for our SF_6 filled cell and x_0 has units of millimeters.

In principle, the fringe shift could have been measured by comparing the fringe pattern with the field on to the pattern with the field turned off, such as Fig. 2(a). However, we found that the reference fringe pattern with the field off at T_C + 1 K changed a small but significant amount over a period of two days. This could have been due to a slight mechanical relaxation or a very small leak. To avoid relying on the absolute position of the reference fringe pattern, we compare the fringe shifts at two distances from the wire and subtract off the slope of the reference pattern. The difference in fringe shift from x_0 = 0.24 mm to x_0 = 0.48 mm computed from Eq. 12 for T_C + 30 mK ,T_C + 10 mK and T_C + 5 mK is Δ N = 0.06, 0.25 and 0.58 respectively. The fringe shift differences measured from Figs. 2(b) to (d) are 0.09, 0.17 and 0.38 respectively with an uncertainty of $\pm$ 0.05 fringes. Despite the crude model for the electric field, we have fair agreement. Finally, we point out that Eq. 12 predicts a positive fringe shift at all points x_0. This would be true if the sample was connected to a large reservoir. Conservation of mass in our cell dictates that the density increase near the wire must be accompanied by a density decrease farther from the wire. A careful comparison between Fig. 2(d) and (a) does indeed confirm that the fringe shift passes through a zero and becomes negative far from the wire, but there is some uncertainty in the reference fringe pattern as noted above.

Electrostriction measurements in 1-g using an identical sample cell were unsuccessful. The electrostriction effect is overwhelmed by effects resulting from the dielectrophoretic force. From Fig. 2 we can see that the temperature must be within approximately 30 mK of T_C to observe the electrostriction effect in our cell. However, in 1-g the density stratification becomes significant within 30 mK of T_C. Turning on the electric field quickly draws the denser fluid toward the wire, thereby masking the electrostriction effect. The inhomogeneous electric field acts like a radially-directed psuedo-gravity, attracting denser fluid.

Figure 3 illustrates a quench step in microgravity from above T_C to below T_C with the electric field on (500 V potential). The SF_6 becomes very turbid as it undergoes spinodal decomposition below T_C (Goldburg, 1983). However, close to the wire, the density of the SF_6 remains above ρ_C, and as liquid condenses it is drawn to the wire. The fluid surrounding the wire never appears to undergo spinodal decomposition. A similar quench with the field turned off did not produce a region of low turbidity around the wire. We can draw an analogy with observations of a quench through T_C in earth's gravity. As the critical point is approached, density stratification causes the fluid to collapse under its own weight resulting in liquid-like densities at the bottom of a container. Within 1 mK of T_C, there is only a very thin region near the mid-height of the cell which is at the critical density. Upon cooling below T_C, the phase transition from one-phase to two-phase is observed only in this thin region. Nothing dramatic happens to the denser fluid at the bottom of the container; it misses the critical point! The same phenomena occurs near the charged wire in microgravity. The excess fluid density in the vicinity of the wire prevents that region from going through the phase transition.

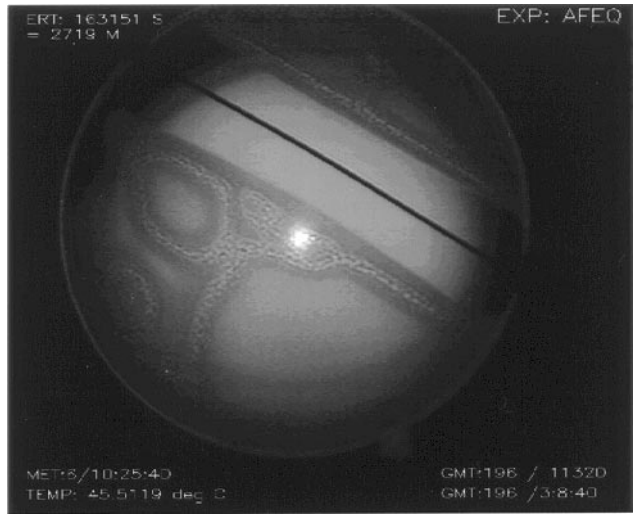

Figure 3.—Image of the visualization cell as T crosses T_C with the 500 V potential on in low-gravity. The turbid fluid was undergoing spinodal decomposition. Near the wire, the fluid did not decompose because it was farther from the critical point due to the increased density. A nonuniform density distribution also existed throughout the cell from a previous quench through T_C, which produced liquid and vapor domains. Note that the fluid had decomposed more where liquid-vapor boundaries ($\rho = \rho_C$) existed from the previous quench. The course-grain structure of these boundary regions signifies a later stage of spinodal decomposition.

All of our observations of electric field effects in the fluid can be qualitatively explained by thinking of the electric field as a radially directed psuedo-gravitational force. For example, in the two-phase region the liquid SF_6 wets the container walls and the shape of the liquid-vapor interface is dominated by surface tension forces. Turning on the electric field in low gravity simply draws the liquid toward the wire. Upon turning the field off, the surface tension forces redistribute the liquid. Any bubbles embedded within the liquid (which we could create by passing a current through the wire) are rapidly displaced by the denser fluid which is drawn in when the electric field is turned on. Turning the field off has no further effect on the bubbles, nor does turning the field back on. This is completely analogous to a thought experiment of turning gravity on and off and watching the motion of a bubble in a container filled with liquid. Initially, the bubble rises to the top and would tend to stay there even if gravity could be turned off and on again.

Just as the electric field can induce flow in the two-phase state, it can also induce convective flow in the single-phase fluid when density (and hence temperature) gradients exist. Such flows were made visible by monitoring the fringe pattern in the IF cell. Turning the electric field on induces flow which subsided within a minute (the viscous relaxation time), and turning the field off and on again resulted in no further action. For a strong enough temperature (and hence density) gradient, the flow is also visible in the visualization

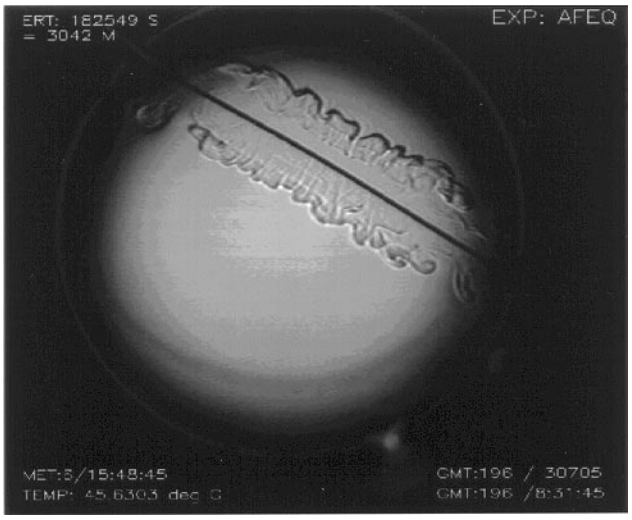

Figure 4.—Convective flow in the visualization cell at T_c+100 mK. The electric field was turned on after creating a low-density region around the wire by using a heat pulse.

cell. Figure 4 shows an example of what appears to be a Rayleigh-Bénard type instability produced in microgravity. At T_c +100 mK, a 14 mJ current pulse was applied to the wire. This creates a low density cylinder of fluid around the wire. Ten seconds later, the 500 V potential was turned on. The radial force produced by the electric field created an instability, and flow took place.

CONCLUSION

We have found that the electrostriction effect in a near-critical fluid does become more pronounced as the critical point is approached due to the diverging compressibility. The increase in density associated with the electrostriction effect near the wire is slow to develop because of the long thermal diffusion times encountered near the critical point. The density increase near the wire has been measured interferometrically, and is found to be in agreement with that calculated from a simplified model. Many of our observations of electric field effects in the fluid are analogous to a gravitational force directed radially towards the wire.

ACKNOWLEDGMENTS

We would like to thank R. Gammon, R. Kusner, W. Johnson, H. Nahra and the entire CPF team for participating in the experiment operations. We are grateful to NASA and ESA, whom made this experiment possible. We also thank K.Y. Min for helpful discussions about electric field effects in binary mixtures. This work was supported by NASA grant NAG3–1395.

REFERENCES

Debye, P. and Kleboth, J. Chem. Phys. Vol. 42, p. 3155, 1965.

Wirtz, D. and Fuller, G.G., Phys. Rev. Lett., Vol. 71, p. 2236, 1993.

Yosida, Y., Phys. Lett, Vol. 65A, p. 161, 1978.

Sengers, J.V., Sengers, J.M.H., in *Progress in Liquid Physics* edited by Croxton, C.A., Wiley, New York, 1978, Chap. 4.

Jany, P. and Straub, J., Int. J. Thermophysics 8, 165, 1987.

Onuki, A., Hao, H., and Ferrell, R.A., Phys. Rev. Vol. A41, p. 2256, 1990.

Boukari, H., Schaumeyer, Briggs, M.E., and Gammon, R.W., Phys. Rev. Vol, A41, p. 2260, 1990.

Moldover, M.R., Sengers, J.V., Gammon, R.W., and Hocken, R.J., Rev. Mod. Phys, Vol. 51, p. 79, 1979.

Stratton, J.A., *Electromagnetic Theory*, McGraw-Hill, New York, 1941, Chap. 2.

Melcher, J.R. and Hurwitz, M.J., Spacecraft and Rockets, Vol. 4, p. 864, 1967.

Hart, J.E., Glatzmaier, G.A., and Toomre, J., J. Fluid Mech., Vol. 173, p. 519, 1986.

Voronel, A.V. and Gitterman, M.Sh., Sov. Phys. JETP, Vol. 28, p. 1306, 1969.

Landau, L.D. and Lifshitz, E.M., *Electrodynamis of Continuous Media*, Vol. 8, section 18 (Pergamon Press) 1984.

Cork, M., Dewandre, T., and Hueser, D., ESA Bulletin Vol. 74, p. 36, 1993.

Goldburg, W.I., in *Light Scattering Near Phase Transitions*, edited by H.Z. Cummins and A.P. Levanyuk, North Holland Publishing Company, 1983, Chap. 9.

REPORT DOCUMENTATION PAGE

Form Approved
OMB No. 0704-0188

1. AGENCY USE ONLY (*Leave blank*)

2. REPORT DATE
April 1995

3. REPORT TYPE AND DATES COVERED
Technical Memorandum

4. TITLE AND SUBTITLE
Electric Field Effects on a Near-Critical Fluid in Microgravity

5. FUNDING NUMBERS
WU–963–50–0A

6. AUTHOR(S)
G. Zimmerli, R.A. Wilkinson, R.A. Ferrell, H. Hao, and M.R. Moldover

7. PERFORMING ORGANIZATION NAME(S) AND ADDRESS(ES)
National Aeronautics and Space Administration
Lewis Research Center
Cleveland, Ohio 44135–3191

8. PERFORMING ORGANIZATION REPORT NUMBER
E–9540

9. SPONSORING/MONITORING AGENCY NAME(S) AND ADDRESS(ES)
National Aeronautics and Space Administration
Washington, D.C. 20546–0001

10. SPONSORING/MONITORING AGENCY REPORT NUMBER
NASA TM–106894
Corrected Copy

11. SUPPLEMENTARY NOTES
Prepared for the National Heat Transfer Conference sponsored by the American Society of Mechanical Engineers, Portland, Oregon, August 5–9, 1995. G. Zimmerli, NYMA, Inc., Engineering Services Division, 2001 Aerospace Parkway, Brook Park, Ohio 44142 (work funded by NASA Contract NAS3–27186); R.A. Wilkinson, NASA Lewis Research Center; R.A. Ferrell and H. Hao, University of Maryland, Center for Theoretical Physics, Department of Physics, College Park, Maryland 20742 (work funded by NASA Grant NAG3–1395); M.R. Moldover, National Institute of Standards and Technology, Thermophysics Division, Gaithersburg, Maryland 20899. Responsible person, R.A. Wilkinson, organization code 6712, (216) 433–2075.

12a. DISTRIBUTION/AVAILABILITY STATEMENT
Unclassified - Unlimited
Subject Category 77

This publication is available from the NASA Center for Aerospace Information, (301) 621–0390

12b. DISTRIBUTION CODE

13. ABSTRACT ***(Maximum 200 words)***
We have studied the effects of an electric field on a sample of SF_6 fluid in the vicinity of the liquid-vapor critical point. We measured the isothermal increase of the density of a near-critical sample as a function of the applied electric field. In agreement with theory, this electrostriction effect diverges near the critical point as the isothermal compressibility diverges. Also as expected, turning on the electric field in the presence of density gradients can induce flow within the fluid, in a way analogous to turning on gravity. These effects were observed in a microgravity environment by using the Critical Point Facility which flew onboard the Space Shuttle Columbia in July 1994 as part of the Second International Microgravity Laboratory Mission. Both visual and interferometric images of two separate sample cells were obtained by means of video downlink. The interferometric images provided quantitative information about the density distribution throughout the sample. The electric field was generated by applying 500 Volts to a fine wire passing through the critical fluid.

14. SUBJECT TERMS
Electrostriction; Critical fluid; Microgravity

15. NUMBER OF PAGES
8

16. PRICE CODE
A02

17. SECURITY CLASSIFICATION OF REPORT
Unclassified

18. SECURITY CLASSIFICATION OF THIS PAGE
Unclassified

19. SECURITY CLASSIFICATION OF ABSTRACT
Unclassified

20. LIMITATION OF ABSTRACT